DOI: 10.1002/ejic.201100407

Cyanide-Bridged Molecular Squares – The Building Units of Prussian Blue

Graham N. Newton,[a] Masayuki Nihei,[a] and Hiroki Oshio*[a]

Keywords: Cyanide ligands / Heterometallic complexes / Spin crossover / Electrochemistry / Electron transfer

Cyanide-bridged molecular squares offer a unique opportunity for study, as they represent a model of the simplest unit of Prussian blue and allow access to a wide range of physical properties that can be monitored, such as rich electrochemistry, valence- and spin-state control, and spin-crossover phenomena. This microreview presents recent findings in the field of cyanide squares with particular focus on their syntheses and physical properties.

Introduction

The study of ferric hexacyanoferrate, or Prussian blue, and its analogues has a long and rich history, which dates back to the start of the 18th century when the earliest records were published.[1] Prussian blue has a face-centered cubic structure in which alternating Fe^{II} and Fe^{III} centers are bridged by cyanide ions in a Fe^{II}–C≡N–Fe^{III} fashion, forming an infinite 3D network. Prussian blue itself is a ferromagnet with a Curie temperature (T_C) of 5.6 K,[2] while some heterometallic derivatives display ferrimagnetism up to room temperature.[3] In fact, the inclusion of heterometals in place of iron has led to the observation of a wide range of physical properties in Prussian blue analogues including photomagnetism, spin crossover, and electrochromicity, which suggests possible uses in hydrogen storage, as molecular sieves, and in nanoscale devices.[4] Due to the structurally infinite nature of Prussian blue and its analogues and the range of their associated properties, there has been much research conducted into the synthesis of discrete analogues; *molecular species*, to investigate the properties of what are essentially Prussian blue fragments. Amongst these fragments, the most prominent may be the octanuclear cube complexes, which have been extensively

[a] Department of Chemistry, Graduate School of Pure and Applied Sciences, University of Tsukuba,
Tennodai 1-1-1, Tsukuba 305-8571, Japan
Fax: +81-29-853-4426
E-mail: oshio@chem.tsukuba.ac.jp

Graham N. Newton was born in 1982 in Edinburgh, UK. He received his M.Sci. (2005) from the University of Glasgow, where he also obtained his Ph.D. (2009) under the guidance of Prof. Lee Cronin. His doctoral studies focused on the synthesis of polynuclear coordination compounds and the use of cold-spray ESI-MS as a means of tracking their assembly and predicting their structure. In 2008 he moved to the University of Tsukuba to work with Prof. Hiroki Oshio on a Japan Society for the Promotion of Science (JSPS) postdoctoral fellowship, investigating the synthesis and properties of high-spin functional clusters and the processes involved in their self-assembly. He was appointed assistant professor in the Oshio group in April 2011.

Masayuki Nihei was born in 1974 in Tokyo. He received his B.S. (1997) from Keio University, and his M.Sci. (1999) and Ph.D. (2002) from the University of Tokyo. His Ph.D. studies, conducted under the supervision of Prof. Hiroshi Nishihara, focused on the creation of photo- and proton-responsive azo-conjugated metalladithiolenes. In 2002 he joined Prof. Hiroki Oshio's group at the University of Tsukuba as an assistant researcher studying the syntheses and magnetic properties of external-stimuli-responsive metal complexes. Working in the Oshio lab, he became a research associate in December 2002, assistant professor in 2005, and associate professor in 2010. His current research centers upon the generation of multinuclear cyanide-bridged clusters and the development of their properties as multi-bistable switchable molecules.

Hiroki Oshio was born in 1953 in Fukuoka. He graduated from Kyushu University in 1977 and obtained his Ph.D. in 1982 under the guidance of Prof. Yoshimasa Takashima. As a postdoctoral fellow, he worked with Prof. Kazuo Nakamoto at Marquette University between 1982 and 1984, before being appointed as a research associate at the Institute for Molecular Science (Okazaki, Japan) in 1985. In 1992 he moved to Tohoku University as an Associate Professor, where he began his studies of cyanide-bridged squares until 2001 which saw him appointed as a Professor at the University of Tsukuba in the Graduate School of Pure and Applied Sciences, where his research has focused on the synthesis and study of magnetic molecules and bistable multinuclear clusters.

 © 2011 Wiley-VCH Verlag GmbH & Co. KGaA, Weinheim

studied,[5] and tetranuclear square clusters, which will be discussed herein. Cyanide-bridged metal complexes are not, however, confined to these architectures, and a huge range of clusters have been reported and shown to possess a wide range of structural topologies and physical properties.[6] This review focuses on cyanide-bridged molecular squares and provides an overview of the syntheses, structures, and physical properties of these materials.

The cyanide-bridged molecular square, which can be considered the simplest model of the infinite Prussian blue structure, was first reported by Schinnerling et al. for a Ti_4 square in 1992,[7] and firstly for a high-spin complex by Oshio et al. in 1999.[8] Since then, there have been many reports of similar structures, both homo- and heterometallic, constructed from both transition metal and closed shell metal ions. This review is concerned primarily with open-shell transition metal ion square complexes. It should also be noted that the clusters referred to in this article as "squares" may often be more accurately described as rectangular or rhombic; however, the term "square" provides us with a simplistic and broadly accurate means of describing their form.

The Synthesis of Cyanide-Bridged Molecular Squares

The general synthetic approach adopted in the preparation of molecular Prussian blue derivatives is to combine solvated metal cations with cyanometalate ions. In order to prevent polymerization it is necessary to employ capping ligands in the syntheses, which will dictate the number and relative position of the available binding sites on the metal ions. For example, a capped cyanometalate mononuclear building block may be added to a solution of solvated metal ions (or of a second capped metal ion) resulting in the crystallization of cyanide-bridged molecular species whose topology is dependent upon the angle between the available binding sites of the cyanometalate ion. Considering square cyanide-bridged molecules, the capped metal ions should have at least two available *cis* binding sites to allow coordination with an angle of approximately 90° between the coordination vectors. These directing building blocks may be octahedral, square pyramidal, or square planar as long as there remain two open binding sites at an appropriate angle to each other.[6,9] The building block approach to the synthesis of cyanide-bridged molecular squares is summarized in Scheme 1.

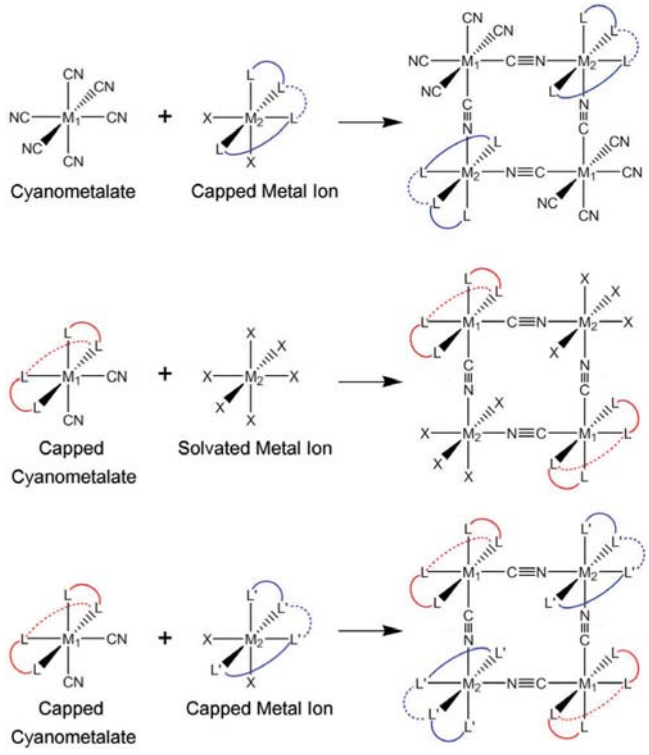

Scheme 1. Three different approaches to the synthesis of cyanide-bridged squares. The red and blue lines represent the behavior of bi- and tetradentate capping ligands.

The successful use of the building block approach in the syntheses of new cyanide-bridged molecular square clusters means that the choice of ligands is critical, and a wide range of ligand systems have been reported as good capping groups, both on the cyanometalate ions and on the solvated metal ions. For example, in the first high-spin examples of cyanide-bridged molecular squares, $\{[(bpy)_2Fe^{II}(CN)_2]_2[Cu^{II}(bpy)]_2\}(PF_6)_4$ and its oxidized derivative $\{[(bpy)_2Fe^{III}(CN)_2]_2[Cu^{II}(bpy)]_2\}(PF_6)_6$,[8] Oshio et al. showed that molecular squares could be controllably isolated by using only 2,2′-bipyridine (bpy) as a capping ligand (Figure 1a). This work was then extended to synthesize the homo- and heterometallic species $\{[(bpy)_2Fe^{II}(CN)_2]_2[M^{II}(bpy)_2]_2\}(PF_6)_4$ [M = Fe, Co,[10] Ru[11]]. It was also shown that a combination of ligands could be used in the synthesis, the tetradentate ligand tris(2-pyridylmethyl)amine (tpa) being used to cap iron ions in conjunction with the $[(bpy)_2Fe^{II}(CN)_2]$ building blocks to form $\{[(bpy)_2Fe^{II}(CN)_2]_2[Fe^{II}(tpa)]_2\}(X)_4$ [X = BF_4[12] or PF_6[13]]. Such capping ligands are not, however, limited to di- and tetradenticity. Some of the most commonly used ligands in the synthesis of cyanide-bridged molecular squares are, in fact, tridentate, such as *i*Prtacn (1,4,7-tris-isopropyl-1,4,7-triazacyclononane)[14] and tp {hydrotris(pyrazol-1-yl)borate}, or tp*, in which the pyrazole groups are dimethyl-derivatized,[15] although often the use of such ligands can lead to the synthesis of cubic M_8 cyanide-bridged clusters. To avoid this, the second metal center is usually capped to ensure that the orientation of its free coordination sites determines the overall cluster topology. This capping of both centers was recently extended to form the hybrid square complex $[Fe_4(\mu\text{-}CN)_4bpmq_4](CN)_2(SeCN)_2$ {bpmq = 2,3-bis[{3-(pyridin-2-yl)-1*H*-pyrazol-1-yl}methyl]quinoxaline}, in which the metals were bridged by both cyanide ions and bpmq groups.[16]

In contrast to this approach, capping only one of the cluster building blocks has also proven a possible method. For example, a heterometallic cyanide-bridged square complex, $\{[tp^*Fe^{III}(CN)_3M^{II}(DMF)_4]_2(OTf)_2\}\cdot 2DMF$ (M^{II} = Mn, Co, Ni), can also be synthesized from the reaction of the $[tp^*Fe(CN)_3]$ building block with DMF-solvated man-

 © 2011 Wiley-VCH Verlag GmbH & Co. KGaA, Weinheim

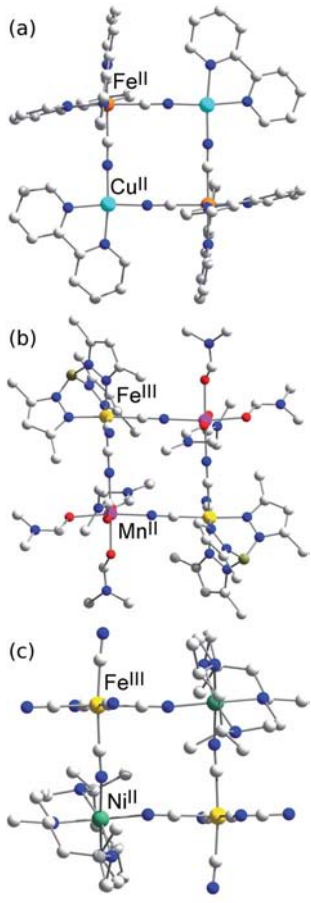

Figure 1. Examples of cyanide-bridged molecular squares: (a) $\{[(bpy)_2Fe^{II}(CN)_2]_2[Cu^{II}(bpy)]_2\}(PF_6)_4$, (b) $\{[Tp^*Fe^{III}(CN)_3Mn^{II}(DMF)_4]_2(OTf)_2\}\cdot 2DMF$, (c) (*meso*-CTH-$H_2$)[$\{Ni(rac\text{-}CTH)\}_2\{Fe(CN)_6\}_2]\cdot 5H_2O$. In all cases, solvent molecules, counterions, and protons have been removed for clarity. Fe^{II} ions are orange; Fe^{III} gold, Cu^{II} light blue, Mn^{II} pink, Ni^{II} green, B gray, C gray, and N blue.

ganese, cobalt, or nickel ions,[17] or even when hexacyanoferrate ($[Fe(CN)_6]^{3+}$) ions are introduced to solvated nickel ions in the presence of the four-coordinate ligand *rac*-CTH (= *rac*-5,7,7,12,14,14-hexamethyl-1,4,8,11-tetrazacyclotetradecane) to form (*meso*-CTH-H_2)[$\{Ni(rac\text{-}CTH)\}_2\{Fe(CN)_6\}_2]\cdot 5H_2O$.[18] In fact, there are a number of examples of square syntheses that use uncapped cyanometalates such as $[W(CN)_8]^{3-/4-}$,[19] $[Ni(CN)_4]^{2-}$[20] and $[Pt(CN)_4]^{2-}$,[21] as well as $[Fe(CN)_6]^{3-}$.[22] Figure 1 gives some examples of cyanide-bridged molecular squares, obtained following different synthetic approaches.

In addition to the wide range of syntheses using labile coordinating ligands, there are a number of examples of squares that use cyclopentadienyl (cp),[23] cyclooctadienyl (cod),[24] and other organometallic capping ligands.[25]

Electrochemistry and Mixed Valence

Prussian blue derivatives often show a very rich and diverse electrochemistry, as a result of the moderately strong electronic coupling interactions that have been observed in many ordered arrays and grid-type complexes[26] and the structure of the cluster possessing adequate stability to accommodate the changes in bond lengths associated with the oxidation and reduction of the metal centers.

Since the Creutz–Taube ion, $[(H_3N)_5Ru(pyr)Ru(NH_3)_5]^{5+}$, was first reported in 1969[27] the scale of the search for new mixed-valence clusters has steadily increased. Much research has been conducted on the properties of mixed-valence-state species and on the way interactions between different metal ions can affect the overall physical properties of a system.[28] Mixed-valence squares are considered to have potential applications in the quantum cellular automata approach to nanoelectronics.[29] Discrete mixed-valence compounds are classified by using the Robin–Day criteria to constitute three main groups of complexes. Class I corresponds to species that show no electronic coupling (localized valence electrons) between metal centers. Class II complexes display a moderate degree of electronic coupling (partial delocalization) between metal centers, which makes the charge formally localized but can also bestow new physical properties such as permitting electron transfer as a result of the application of external stimuli. The final class of species, Class III, includes complexes in which very strong electronic coupling (complete delocalization) between metal centers ensures that the metal centers in a complex cannot be considered to have integer oxidation states, rather an average of the oxidation state of the coupled metal ions.[30]

To investigate the redox properties of cyanide-bridged molecular squares, cyclic voltammetry (CV) measurements were conducted on a $[Fe_4(\mu\text{-}CN)_4(bpy)_8](PF_6)_4\cdot 4H_2O$ ($[Fe^{II}_4]^{4+}$) square and its heterometal derivative $[Fe_2Co_2]^{4+}$.[10] The CV data of the $[Fe^{II}_4]^{4+}$ cluster {whose core can be described as [Fe(CN)Fe(NC)Fe(CN)Fe(NC)]$^{n+}$} included quasireversible waves at 0.67 (ΔE_p = 70 mV) and 0.86 V (ΔE_p = 80 mV) vs. SSCE, followed by an irreversible wave at 1.37 V. Coulomb potentiometry conducted at 1.0 V revealed that the quasireversible waves corresponded to two one-electron redox processes. In the $[Fe^{II}_4]^{4+}$ cluster core, the Fe^{2+} ions interact with either cyanide carbon or nitrogen atoms, and the donor atoms determine the sites of the redox processes. The Fe–C bond stabilizes the d orbitals of the metal center through π back-donation, while the σ-donating character of the cyanide N terminal dictates that the Fe–N interaction destabilizes the associated metal center d orbitals, allowing oxidation to occur. Thus, the quasireversible oxidation steps occur at the Fe^{2+} ions and are coordinated by the cyanide nitrogen atoms. In terms of the cluster core, the first two-step redox behavior can be interpreted as shown in Equation (1).

$$[Fe^{II}(CN)Fe^{II}(NC)Fe^{II}(CN)Fe^{II}(NC)]^{4+} \underset{+e}{\overset{-e}{\rightleftharpoons}} [Fe^{II}(CN)Fe^{III}(NC)Fe^{II}(CN)Fe^{II}(NC)]^{5+} \underset{+e}{\overset{-e}{\rightleftharpoons}} [Fe^{II}(CN)Fe^{III}(NC)Fe^{II}(CN)Fe^{III}(NC)]^{6+} \quad (1)$$

The potential difference between the two one-electron oxidation processes is indicative of the stability of the $[Fe^{II}_3Fe^{III}]^{5+}$ species, which is imparted by electron delocal-

 © 2011 Wiley-VCH Verlag GmbH & Co. KGaA, Weinheim

ization. The comproportionation constant provides a means of quantifying this mixed-valence stability and can be calculated from Equation (2).

$$[Fe^{II}(CN)Fe^{II}(NC)Fe^{II}(CN)Fe^{II}(NC)]^{4+} + [Fe^{II}(CN)Fe^{III}(NC)Fe^{II}(CN)Fe^{III}(NC)]^{6+} \underset{}{\overset{K_c}{\rightleftharpoons}} 2[Fe^{II}(CN)Fe^{III}(NC)Fe^{II}(CN)Fe^{II}(NC)]^{5+} \quad (2)$$

The observed potential difference (ΔE = 0.19 V) corresponds to a comproportionation constant of $K_c = 2.4 \times 10^3$, which suggests a moderately high thermodynamic stability for the $[Fe^{II}_3Fe^{III}]^{5+}$ species. In contrast, the potential difference between the second oxidation wave (5+ to 6+) and the third (irreversible) step is far greater, ΔE = 0.51 V. The size of the observed potential difference can be justified as a combination of two factors: the asymmetry of the bridging cyanide ligands and the occurrence of inter-valence charge transfer (IVCT) electron delocalization. The electronic spectrum of $[Fe^{II}_4]^{4+}$ in acetonitrile at –30 °C showed, with the formation of the mono- ($[Fe^{II}_3Fe^{III}]^{5+}$) and subsequent di-oxidized $[Fe^{II}_2Fe^{III}_2]^{6+}$ mixed-valence species, the increase in intensity of a new band in the NIR region. The band (λ_{max} = 1380 nm, ε_{max} = 8600 $M^{-1}cm^{-1}$) was assigned as an IVCT transition from the C-coordinated Fe^{II} ions to the N–Fe^{III} centers in the $[Fe^{II}_2Fe^{III}_2]^{6+}$ state. Hush theory[31] was used to derive the IVCT parameters based on ε_{max} = 4300 $M^{-1}cm^{-1}$ (two chromophores), $\tilde{\nu}_{max}$ = 7250 cm^{-1} (1380 nm), and $\Delta\nu_{1/2}$ = 1450 cm^{-1}, giving an electronic interaction matrix element, H_{ab} = 870 cm^{-1}, and an electron delocalization degree, α^2 = 0.014, which are in accordance with a Class II assignment of the mixed-valence cluster.

This work was logically extended to investigate the heterometallic square $[Ru^{II}_2Fe^{II}_2(\mu\text{-}CN)_4(bpy)_8]^{4+}$ ($[Ru^{II}_2Fe^{II}_2]^{4+}$), which has a core connectivity of [Ru(CN)Fe(NC)-Ru(CN)Fe(NC)]$^{n+}$.[11] Ru^{II} centers occupied the C-bonding positions, allowing further redox states to be accessed, four one-electron-oxidized species being observed electrochemically in acetonitrile: $[Ru^{II}_2Fe^{II}_2]^{4+} \rightleftharpoons [Ru^{II}_2Fe^{II}Fe^{III}]^{5+} \rightleftharpoons [Ru^{II}_2Fe^{III}_2]^{6+} \rightleftharpoons [Ru^{II}Ru^{III}Fe^{III}_2]^{7+} \rightleftharpoons [Ru^{III}_2Fe^{III}_2]^{8+}$ (with waves at 0.69, 0.84, 1.42, and 1.70 V vs. SSCE respectively; see Figures 2 and 3 and Table 1).

The first two waves observed (0.69 and 0.84 V) are a very good match to those seen in the $[Fe^{II}_4]^{n+}$ sample (0.67 and 0.86 V), which were demonstrated to indicate the oxidation

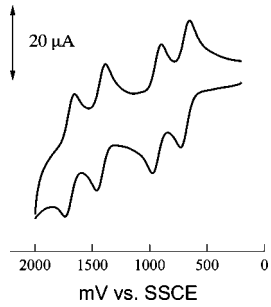

Figure 2. CV of $[Ru^{II}_2Fe^{II}_2(\mu\text{-}CN)_4(bpy)_8](PF_6)_4$ in CH_3CN containing 0.1 M $[Bu_4N]PF_6$ collected at a scan rate of 100 mV s^{-1} at 20 °C.

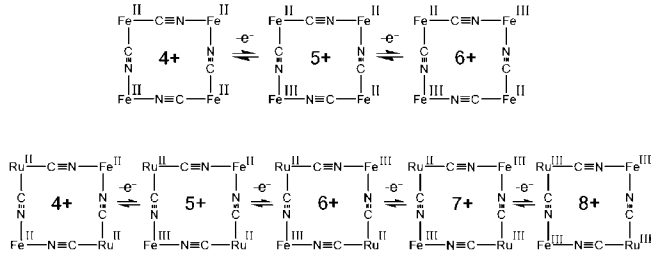

Figure 3. Schematic summary of the redox species observed in the CV spectra of $[Fe_4]^{n+}$ (top) and $[Ru_2Fe_2]^{n+}$ (bottom).

of the N-coordinated Fe^{II} centers to Fe^{III}. Therefore, the corresponding steps in $[Ru^{II}_2Fe^{II}_2]$ can be assumed to represent the oxidation of the iron ions. The first two oxidation waves are followed by a large gap, before a second pair of one-electron processes are observed at high potential (1.42 and 1.70 V), which can be assigned as the stepwise oxidation of the ruthenium ions. The observed potential differences for the mixed-valence species $[Ru^{II}_2Fe^{II}Fe^{III}]^{5+}$ and $[Ru^{II}Ru^{III}Fe^{III}_2]^{7+}$ allow the calculation of the K_c values from Equations (3) and (4).

$$[Ru^{II}_2Fe^{II}_2]^{4+} + [Ru^{II}_2Fe^{III}_2]^{6+} \underset{}{\overset{K_c}{\rightleftharpoons}} 2[Ru^{II}_2Fe^{II}Fe^{III}]^{5+} \quad (3)$$

$$[Ru^{II}_2Fe^{III}_2]^{6+} + [Ru^{III}_2Fe^{III}_2]^{8+} \underset{}{\overset{K_c}{\rightleftharpoons}} 2[Ru^{II}Ru^{III}Fe^{III}_2]^{7+} \quad (4)$$

Potential differences of ΔE = 0.25 and 0.28 V yield K_c values of 1.7×10^4 and 5.4×10^4 for $[Ru^{II}_2Fe^{II}Fe^{III}]^{5+}$ and

Table 1. CV data for $[Ru^{II}_2Fe^{II}_2]^{4+}$, $[Fe^{II}_4]^{4+}$, and related compounds.[11]

Compound	$E_{1/2}$[a]	Assigned transition	K_c
$[Ru^{II}(CN)_2(bpy)_2]$	0.83	Ru^{II}/Ru^{III}	
$[Fe^{II}(CN)_2(bpy)_2]$	0.47	Fe^{II}/Fe^{III}	
$[Ru^{II}_2Fe^{II}_2(\mu\text{-}CN)_4(bpy)_8](PF_6)_4$	0.69	$Ru^{II}_2Fe^{II}_2/Ru^{II}_2Fe^{II}Fe^{III}$	1.7×10^4
	0.84	$Ru^{II}_2Fe^{II}Fe^{III}/Ru^{II}_2Fe^{III}_2$	
	1.42	$Ru^{II}_2Fe^{III}_2/Ru^{II}Ru^{III}Fe^{III}_2$	
	1.70	$Ru^{II}Ru^{III}Fe^{III}_2/Ru^{III}_2Fe^{III}_2$	5.4×10^4
$[Fe^{II}_4(\mu\text{-}CN)_4(bpy)_8](PF_6)_4$	0.67	$Fe^{II}_4/Fe^{II}_3Fe^{III}$	2.4×10^3
	0.86	$Fe^{II}_3Fe^{II}/Fe^{II}_2Fe^{III}_2$	

[a] Volts vs. SSCE, with a glassy carbon working electrode, in CH_3CN containing 0.1 M $[Bu_4N]PF_6$, collected at a scan rate of 100 mV s^{-1} at 20 °C.

 © 2011 Wiley-VCH Verlag GmbH & Co. KGaA, Weinheim

$[Ru^{II}Ru^{III}Fe^{III}_2]^{7+}$, respectively. These values indicate intermediate thermodynamic stability for the mixed-valence species.

UV/Vis measurements on $[Ru^{II}_2Fe^{II}_2]^{4+}$ showed that the spectrum was dominated by π-to-π* transitions of the bpy ligands and by metal-to-ligand charge transfer (MLCT, d to π*) transitions (λ_{max} = 500 nm with ε = 17400 $M^{-1}cm^{-1}$). The spectra of the $[Ru^{II}_2Fe^{II}Fe^{III}]^{5+}$ and $[Ru^{II}_2Fe^{III}_2]^{6+}$ species were then collected at 0.8 and 1.2 V respectively, to ensure complete transition to the desired oxidized states. On electrochemical one-electron oxidation, the MLCT band shifted towards the blue region and decreased in intensity (λ_{max} = 470 nm with ε = 13100 $M^{-1}cm^{-1}$) whilst showing the growth of a new band in the near-IR region (λ_{max} = 2350 nm with ε = 5500 $M^{-1}cm^{-1}$). Further oxidation at 1.2 V results in a large shift in the MLCT band, again combined with a decrease in intensity (λ_{max} = 410 nm with ε = 10900 $M^{-1}cm^{-1}$) and the appearance of another new band at 1380 nm (ε = 8600 $M^{-1}cm^{-1}$). The new bands can be assigned as IVCT transitions between Fe^{II}–Fe^{III} (2350 nm) and Ru^{II}–Fe^{III} (1380 nm), respectively (Figure 4).

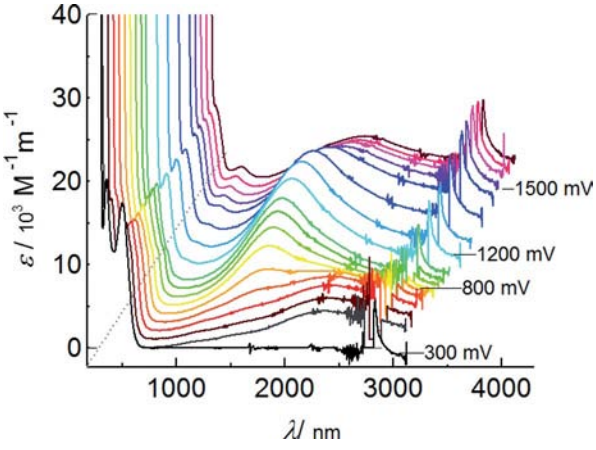

Figure 4. Electronic absorption spectra of $[Ru^{II}_2Fe^{II}_4(\mu\text{-}CN)_4(bpy)_8](PF_6)_4{\cdot}CHCl_3{\cdot}H_2O$. Measurements were conducted at –30 °C in an optically transparent thin-layer electrode consisting of a platinum grid between the windows of a 2 mm spectrophotometric cell. Electrochemical oxidations were carried out with an SSCE reference electrode and a Pt wire counterelectrode separated from the cathodic compartment by a glass frit.

Hush calculations give H_{ab} and α^2 values of 1090 cm^{-1} and 0.065 for $[Ru^{II}_2Fe^{II}Fe^{III}]^{5+}$ and 1990 cm^{-1} and 0.096 for $[Ru^{II}_2Fe^{III}_2]^{6+}$, respectively, indicating a larger degree of electronic delocalization than that observed in the homometallic $[Fe^{II}_2Fe^{III}_2]^{6+}$ cluster (0.014); however, the same assignment as Robin–Day Class II still applies.

Spin-State Control

Cyanide bridges are useful ligands for the construction of high-spin molecules with predictable magnetic interactions.[6] Heterometallic clusters can be controllably made, and the magnetic interactions between metal centers can be related back to the Goodenough–Kanamori rule.[32] For example, interactions between low-spin (LS) Fe^{III} (t_{2g}^5) and high-spin (HS) Mn^{II} ($t_{2g}^3e_g^2$) are predicted to be antiferromagnetic because of the interaction of half-filled orbitals (unpaired spins) through the ligand π-system when considering idealized octahedral geometries. Of course, deviations from the ideal geometries and coordination environments are expected in polynuclear metal clusters, and they lead to complications in the prediction of the interactions; however, the rule acts as a useful basis for discussing the magnetic behavior in cyanide-bridged square systems.

When considering the magnetic properties of cyanide-bridged square polynuclear metal clusters, the Goodenough–Kanamori rule can be very useful, and it provides a means of generating clusters with desirable spin ground states. Of course, using diamagnetic Fe^{II} ions in a square complex results in a spin ground state of the sum of the two uncoupled heterometal spins [Figure 5(a)]. However, focusing on high-spin clusters, and in particular squares containing LS Fe^{III}, a great deal of spin-state control can be gained through the selection of the heterometal ions. For example, in the first report of a fully paramagnetic cyanide-bridged square, $\{[(bpy)_2Fe^{III}(CN)_2]_2[Cu^{II}(bpy)]_2\}(PF_6)_6$, previously discussed, in which two LS Fe^{III} ions were coupled with two Cu^{II} centers, the cluster displayed ferromagnetic interactions and thus a spin ground state of S = 2 (Figure 5).[8] Indeed, this work has been expanded in further studies that have also shown evidence of the LS Fe^{III}/Cu^{II} combination leading to S = 2 squares.[22b,33] Such predictability of the spin state also applies to squares in which the corner sites are shared alternately by LS Fe^{III} and Ni^{II} ions (t_{2g}^5 and $t_{2g}^6e_g^2$, respectively), which almost invariably result in ferromagnetically coupled S = 3 [2 × (1/2) + 2 × (1)] units.[17a,18,34] Likewise, LS Fe^{III}/HS Mn^{II} ($t_{2g}^3e_g^2$) squares provide a means of accessing S = 4 spin ground states, although in this case the ground state results from the antiferromagnetic interaction of two S = 1/2 Fe^{III} centers and two S = 5/2 Mn^{II} ions.[15a,17b]

Dunbar et al. were able to access such a range of spin states in their elegant work on the $\{[M^{II}Cl_2]_2[Co^{II}(triphos)(CN)_2]_2\}$ [M = Mn, Fe, Co, Ni, Zn; triphos = 1,1,1-tris(diphenylphosphanylmethyl)ethane] cyanide-bridged square system.[35] Squares with composition $[Co_2Mn_2]$, $[Co_2Fe_2]$, $[Co_2Co_2]$, $[Co_2Ni_2]$, and $[Co_2Zn_2]$ were synthesized and found to display antiferromagnetic interactions between all (paramagnetic) metal centers and the ever-present LS Co^{II} ions, adhering to the spin-coupling model $S_{total} = S_{M^{II}1} - S_{Co1} + S_{M^{II}2} - S_{Co2}$. This behavior led to a stepwise series of spin ground states where $S_{[CoMn]}$ = 4, $S_{[CoFe]}$ = 3, $S_{[CoCo]}$ = 2, $S_{[CoNi]}$ = 1, and $S_{[CoZn]}$ = 2 × 1/2. An interesting comparison to the Co(triphos) series was reported by Mallah's group in the form of a square with an S = 5 spin ground state. In this case, Ni^{II} and Cr^{III} ions were combined to create a cyanide-bridged square with the formula $\{[i\text{PrtacnCr}(CN)_3Ni(Me_2bpy)_2]_2\}(ClO_4)_4{\cdot}2CH_3CN$ (*i*Prtacn = 1,4,7-tris-isopropyl-1,4,7-triazacyclononane, Me_2bpy = 4,4-dimethyl-2,2-bipyridine). The mixed Ni^{II}/Cr^{III} system displayed ferromagnetic interactions between metal centers, leading to an S = 5 ground state.[14]

 © 2011 Wiley-VCH Verlag GmbH & Co. KGaA, Weinheim

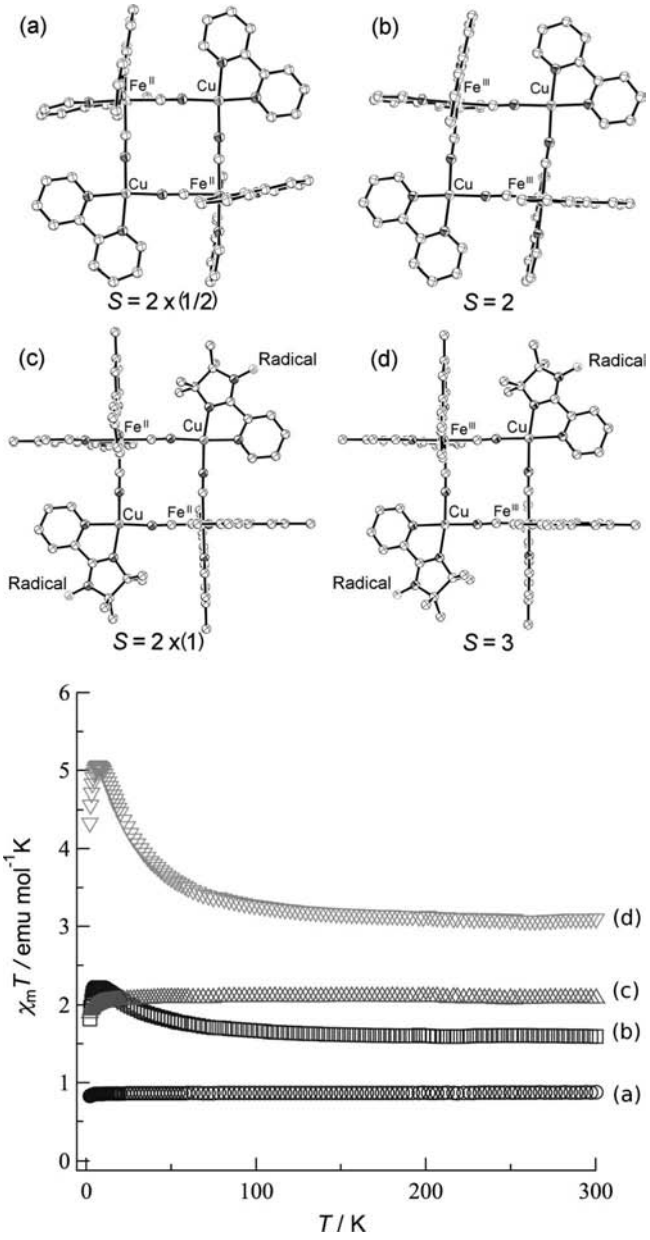

Figure 5. ORTEP diagrams and susceptibility data for four $[Fe_2Cu_2]^{n+}$ squares: (a) $[Fe^{II}_2Cu^{II}_2]^{4+}$, (b) $[Fe^{III}_2Cu^{II}_2]^{6+}$, (c) $[Fe^{II}_2Cu^{II}_2Radical_2]^{4+}$, and (d) $[Fe^{III}_2Cu^{II}_2Radical_2]^{6+}$.

First-row transition metal ions are not the only possible constituents of cyanide-bridged molecular squares and related materials. There are also several examples of transition metal/lanthanide mixed metal clusters in which weak magnetic interactions can be observed between the metal centers.[36] For example, a study by Kou et al. published in 2002 reported the synthesis and properties of a Cr_2Gd_2 square with an $S = 4$ spin ground state resulting from weak antiferromagnetic interactions between two $S_{Gd} = 7/2$ Gd^{III} ions and two $S_{Cr} = 3/2$ Cr^{III} centers. High-field magnetic measurements showed that spin-flip occurred, switching the ferrimagnetic cluster to the ferromagnetic form.

A further approach to asserting control over the spin ground states of cyanide-bridged squares was reported in an $[Fe^{III}_2Cu^{II}_2]$ square in which imino nitroxide ligands were used.[37] The Fe^{III} ions were in the low spin state, and thus ferromagnetic interactions could be predicted to be operative between metal centers, suggesting that the square should conform to the expected $S = 2$ spin ground state. However, the imino nitroxide radical ligand was shown to couple through very strong ferromagnetic interactions ($J > 300$ K) with the doublet spin of the coordinated Cu^{II} ion due to the strict orthogonal arrangement of the Cu^{II} ($d_{x^2-y^2}$) and imino nitroxide magnetic orbitals (π^*), meaning that both Cu^{II} centers could be treated as effective triplet species. The subsequent interaction between the Cu^{II} $d_{x^2-y^2}$ orbitals and the neighboring doublet spins of the Fe^{II} $d\pi$ orbitals meant that the overall spin ground state was $S = 3$ as a result of the ferromagnetic interaction of the three distinct paramagnetic centers. The corresponding result was also obtained from the complex when the iron ions were in the diamagnetic LS Fe^{II} state. The magnetic susceptibility data showed that the Cu^{II} ions were ferromagnetically coupled to the radicals, which resulted in a spin ground state of $S = 2 \times (1)$ (Figure 5).

Such control of the magnetic spin ground state in cyanide-bridged paramagnetic clusters through the choice of transition metals also has further applications in determining the magnetic properties of cyanide-bridged square complexes. For example, the combination of Fe^{III} and Ni^{II} ions in heterometallic squares has led to numerous examples of clusters displaying single molecule magnet (SMM) type behavior.[17a,33a,34] The source of the anisotropy, requisite for all SMMs, in $[Fe_2Ni_2]^{6+}$ squares was investigated by Park et al. in relation to a second cyanide-bridged square SMM, $[Fe_2Co_2]^{6+}$, and it was shown that the majority of the cluster anisotropy originated from the LS Fe^{III} ions as a result of spin–orbit coupling. In contrast, the primary source of anisotropy in the $[Fe_2Co_2]^{6+}$ example was shown to be the significant spin–orbit coupling in the Co^{II} centers.[38] This finding was later supported by further studies by Clérac et al., which showed that the SMM behavior of two $[Fe_2Ni_2]^{6+}$ square complexes was independent of the degree of distortion around the Ni^{II} centers and arose primarily from the orbital contribution of the Fe^{III} ions.[34a]

Spin Crossover

The spin-crossover (SCO) phenomenon occurs when the application of an external stimulus to a material in which a metal center exists in a ligand field of appropriate strength causes the metal ion to make a transition between the HS and LS phase. This potential for bistability, that is, a system exhibiting two phases at a given temperature, means that it is one of the major fields of research in the search for molecular devices that can act as single molecular switches.[39] Cyanide groups can be useful ligands in SCO complexes, and numerous examples of cyanide coordinated SCO metal centers have been reported. SCO complexes are still most commonly low-nuclearity species, and there are as yet very few examples of cyanide-bridged squares that display this

 © 2011 Wiley-VCH Verlag GmbH & Co. KGaA, Weinheim

trait. The first reported example was presented by the Oshio group,[13] in which an Fe_4 square could be tuned to display SCO behavior. Previous studies on the $[Fe_2M_2(\mu\text{-}CN)_4(bpy)_8]^{n+}$ molecular squares (M = late-first-row transition metal ion)[10] led to diamagnetic clusters when Fe^{II} ions were used; however, by replacing bpy with tris(2-pyridylmethyl)amine (tpa), the ligand-field strength on the Fe^{II} centers could be weakened, and the resulting ferrous square, $[Fe^{II}_4(\mu\text{-}CN)_4(bpy)_4(tpa)_2](PF_6)_4$ {$[Fe_4(tpa)_2]$, Figure 6}, showed a two-step spin transition.

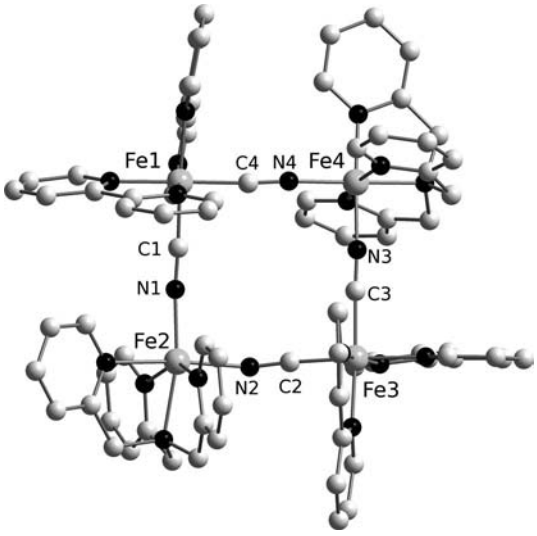

Figure 6. Diagram of $[Fe_4(tpa)_2]$ at 200 K. Average coordination bond lengths (in Å) of Fe^{II} ions at 100 K: Fe1 1.958, Fe2 1.976, Fe3 1.958, Fe4 1.963; at 200 K: Fe1 1.954, Fe2 2.154, Fe3 1.955, Fe4 1.965; and at 300 K: Fe1 1.954, Fe2 2.165, Fe3 1.959, Fe4 1.968.

Single-crystal X-ray diffraction data collected at 100 K led to the elucidation of a structure in which all four Fe^{II} centers had very similar bond lengths, within the range 1.958–1.976 Å, characteristic of LS Fe^{II} ions. X-ray structures determined at 200 and 300 K showed that three of the Fe^{II} ions (Fe1, Fe3, and Fe4) remained in the LS state, while the bonding distances around Fe2 extended to between 2.154 and 2.165 Å, indicative of HS Fe^{II}.

Magnetic susceptibility measurements were carried out in the range 5–400 K, and the results are shown in Figure 7. The $\chi_m T$ value below 100 K was constant and near zero (0.3 emu mol^{-1} K), in line with the predicted diamagnetic state of four LS Fe^{II} ions, albeit with a paramagnetic impurity that corresponded to 2.5% of the HS Fe^{II}, $S = 2$ species. As the temperature increased to 200 K, the $\chi_m T$ values rose to a plateau value at 3.2 emu mol^{-1} K, close to the value (3.0 emu mol^{-1} K) expected for an isolated HS Fe^{II} ion. The plateau has a width of approximately 100 K, centered around 240 K. Subsequent temperature increase induced a second spin-crossover event; however, the $\chi_m T$ values did not reach the expected plateau value (6.0 emu mol^{-1} K) for two independent HS Fe^{II} ions. At the highest temperature measured (400 K), the $\chi_m T$ value was 4.9 emu mol^{-1} K, corresponding to 57% conversion of the Fe4 centers into the HS state.

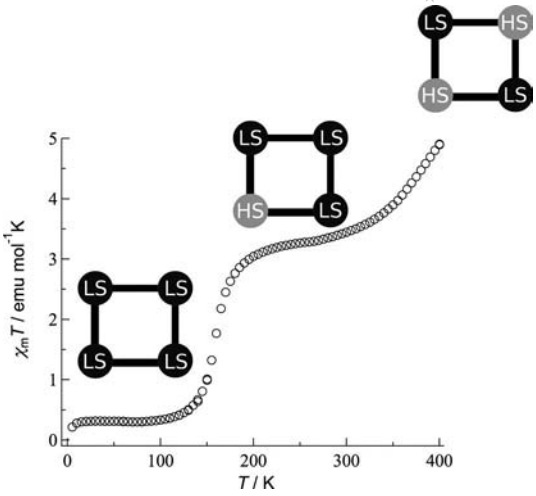

Figure 7. Magnetic susceptibility data collected for $[Fe_4(tpa)_2]$ between 5 and 400 K, with schematics representing the spin transition in the squares.

The spin-crossover behavior of $[Fe_4(tpa)_2]$ was further supported by ^{57}Fe Mössbauer spectroscopic data collected across a wide temperature range, summarized in Figure 8. The Mössbauer spectrum at 50 K was dominated by two doublets characteristic of LS Fe^{II} species, although a low-intensity signal characteristic of HS Fe^{II} species could also be seen due to a paramagnetic impurity. The LS1 and LS2 doublets were assigned to the Fe1/Fe3 and Fe2/Fe4 pairs, respectively. The peak-area ratio of the LS1, LS2, and HS doublets was 0.52:0.44:0.04 at 50 K. As the temperature was increased, the LS2 doublet lost intensity, and the HS doublet gained intensity leading to peak area ratios for LS1,

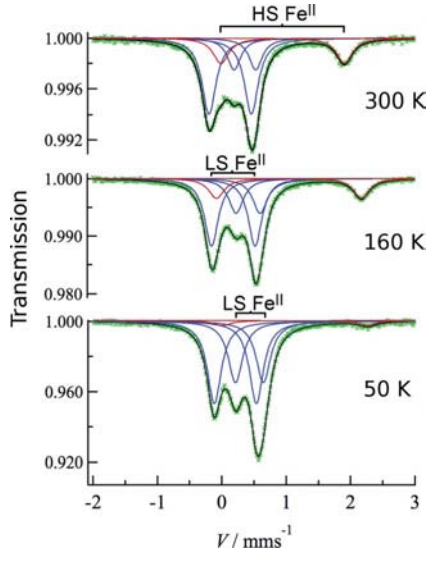

Figure 8. Mössbauer spectra of $[Fe_4(tpa)_2]$ collected at 50, 160, and 300 K showing observed (green crosses), fit (black lines), LS doublets (blue lines), and HS doublets (red lines). Transmission values are relative and velocity (V) is relative to metallic iron. At 50 K: blue lines, LS1: $\delta = 0.21$ and $\Delta E_Q = 0.66$ mm s^{-1}; LS2: $\delta = 0.43$ and $\Delta E_Q = 0.43$ mm s^{-1} and red line, $\delta = 1.13$ and $\Delta E_Q = 2.26$ mm s^{-1}.

 © 2011 Wiley-VCH Verlag GmbH & Co. KGaA, Weinheim

LS2, and HS doublets of 0.53:0.29:0.18 and 0.56:0.22:0.21 at 160 and 300 K, respectively, suggesting that either Fe2 or Fe4 had adopted the HS state at 300 K.

In later work on the same system, Nihei et al. showed that by replacing the tpa ligands with 2,2′-bipyrimidine (bpym) to form a square of formula $[Fe^{II}_4(\mu\text{-}CN)_4(bpy)_4(bpym)_4](PF_6)_4\cdot 6MeOH\cdot 4H_2O$, $[Fe_4(bpym)_4]$, the two-step nature of the SCO process was replaced by a one-step transition.[40] Once more, complete transition could not be observed up to 400 K, at which temperature the $\chi_m T$ value was 3.42 emu mol^{-1} K, corresponding to 57% conversion of the bpym-coordinated iron ions to the HS state. This work was further developed by Boldog et al., who reported that the properties of the Fe_4 square could be similarly altered to show one-step SCO behavior by replacing the bpy ligands with 1,10-phenanthroline (phen) groups to form $[Fe_4(\mu\text{-}CN)_4(phen)_4(tpa)_2](PF_6)_4$, $[Fe_4(phen)_4]$.[41] The observed differences in the spin transition behavior between the three complexes show the need for the subtle balance of structural factors to generate multiple-step SCO species. These differences in behavior between Fe4 cyanide squares was recently investigated from a theoretical viewpoint by Zueva et al. with the conclusion that the observation of multistep SCO was purely the influence of asymmetrical crystal packing.[42] The $[Fe_4(tpa)_2]$ cluster had triclinic symmetry, and thus four crystallographically distinct metal coordination sites, one of which (Fe2) had a substantially distorted octahedral coordination environment due to very strong π–π interactions between the coordinating tpa ligand and that of the Fe2 ion on a neighboring cluster. This occurrence led to a decrease in the ligand field strength around Fe2 and, in turn, to the two-step SCO. $[Fe_4(bpym)_4]$, like $[Fe_4(tpa)_2]$, crystallized in the triclinic space group, $P\bar{1}$; however, the square had a pseudo-inversion center and showed no substantial distortion or asymmetrical intermolecular interactions. Likewise, the $[Fe_4(phen)_4]$ cluster crystallized with monoclinic symmetry, ensuring that the SCO-active Fe^{II} ions were crystallographically identical and the ligand fields were equivalent. It is interesting to note that the spin transition in $[Fe_4(phen)_4]$ begins somewhere around 300 K, almost the same temperature as the second transition in $[Fe_4(tpa)_2]$. This suggests that the nondistorted Fe4 center in $[Fe_4(tpa)_2]$ shows what may be considered to be the expected SCO susceptibility for a $[Fe^{II}tpa(NC)_2]$ center.

The Fe_4 square system is not the only example of SCO behavior in cyanide-bridged molecular squares. In 2006 Colacio's group observed spin transition in a heterometallic $[Fe^{II}_2Ni^{II}_2]$ square, $\{[Ni(rac\text{-}zTH)]_2[Fe(CN)_2(bpy)_2]_2\}(ClO_4)_4\cdot H_2O$, in which the end of a transition from HS to LS Fe^{II} centers can be seen below 400 K. The cluster reached the LS state, and thus the overall paramagnetic $S = 2\times 1$ ground state of two non-interacting Ni^{II} ions below 240 K.[18]

Electron-Transfer-Coupled Spin Transition

Recently there has been much research conducted into the charge-transfer behavior associated with heterometallic cyanide-bridged materials and molecules. The so-called charge-transfer-induced spin transition (CTIST)[43] was first observed in Prussian blue analogues by Sato et al. for the compound $K_{0.2}Co_{1.4}[Fe(CN)_6]\cdot 6.9H_2O$, which showed electron transfer from Co^{II} to Fe^{III} ions followed by subsequent transition from HS to LS on the Co^{III} ions. The CTIST behavior was induced by light irradiation of the material's IVCT band.[44] Since that time, there has been much focus on the development of molecular species that display CTIST behavior, by either thermal or photostimulation.

Photoinduced CTIST (from the LS to the light-induced HS phase) follows a multistep pathway; firstly charge transfer from the $[LSFe^{II}LSCo^{III}]$ to the $[LSFe^{III}LSCo^{II}]$ state, causing the metal centers to exist as doublet Fe^{III} and Co^{II} ions. Secondly, the doublet Co^{II} ion undergoes spin transition to reach the HS state of $[LSFe^{III}HSCo^{II}]$. In contrast to the photoinduced process, thermal CTIST is entropy-driven and occurs in one step, that is, electron transfer does not "induce" the spin transition. In this context, the term CTIST succinctly describes the photoinduced phenomenon, but is slightly less accurate in its depiction of the thermal process. Additionally, the term "charge transfer" is used freely to describe cases where a fraction of the electronic charge is shared between two sites ($[AB]\rightleftharpoons[A^+B^-]$) or when a complete transfer of charge has occurred with no delocalization ($[AB]\rightarrow[A^+B^-]$), and as such carries a degree of ambiguity. In CTIST, the $[LSFe^{III}HSCo^{II}]$ state, generated from $[LSFe^{II}LSCo^{III}]$ via the $[LSFe^{III}LSCo^{II}]$ state, can be considered to have no delocalized electrons between the Fe and Co centers, that is, completely localized electron transfer has occurred ($[AB]\rightarrow[A^+B^-]$). Thus, it may be commensurate to term this process electron transfer. In the case of molecular species such as ours, we therefore propose that both the thermal and light-induced processes may be described as electron-transfer-coupled spin transition (ETCST).

Dunbar and co-workers developed a family of pentanuclear cyanometalates of the general formula $\{[M(tmphen)_2]_3[M'(CN)_6]_2\}$, (tmphen = 3,4,7,8-tetramethyl-1,10-phenanthroline), which displayed a range of physical properties such as SMM behavior, linkage isomerism, and SCO, depending on the constituent metal ions. In the mixed-valence $\{[Co(tmphen)_2]_3[Fe(CN)_6]_2\}$ species, they reported the occurrence of thermal CTIST,[45] as they did in their recent study on the osmium-containing cluster $\{[Fe(tmphen)_2]_3[Os(CN)_6]_2\}$.[46] Mixed-valence Fe–CN–Co systems have two accessible electronic states; [LS Fe^{III} (t_{2g}^5)–CN–HS Co^{II} ($t_{2g}^4e_g^2$)] and [LS Fe^{II} (t_{2g}^6)–CN–LS Co^{III} (t_{2g}^6)], which can be accessed at high and low temperature, respectively, and are generated by electron transfer between the iron t_{2g} and the cobalt e_g orbitals. In 2007, Holmes's group, in collaboration with Clérac and Mathonière, reported the first cyanide-bridged molecular cube, $\{[(pzTp)Fe(CN)_3]_4[Co(pz)_3CCH_2OH]_4\}(ClO_4)_4\cdot 13DMF\cdot 4H_2O$ {where pzTp and $(pz)_3CCH_2OH$ were pyrazole-derivatized tridentate ligands}, which exhibited both thermally and light-induced electron transfer processes that led to spin transition.[47] In 2010, the same group published a paper reporting the ob-

 © 2011 Wiley-VCH Verlag GmbH & Co. KGaA, Weinheim

servation of this behavior in a cyanide-bridged molecular square.[48] It should be noted that all previously reported cases of the phenomenon, in molecular and bulk species, have shown one-step transitions. However, the Oshio group recently reported the first example of an ETCST-active complex that showed two-step behavior, and a metastable intermediate state.[49]

An $[Fe_2Co_2]$ square system $[Co_2Fe_2(CN)_6(tp^*)_2(dtbbpy)_4](PF_6)_2{\cdot}2MeOH$ ($[Co_2Fe_2$-1], dtbbpy = 4,4′-di-*tert*-butyl-2,2′-bipyridine) was reported, and X-ray crystal structure analysis for $[Co_2Fe_2$-1] was performed at 100 K. The resultant structure is displayed in Figure 9. $[Co_2Fe_2$-1] is a heterometallic square, in which Fe and Co ions are alternately bridged by cyanide ions. The complex crystallized in the monoclinic space group, *C*2/*c*, where a twofold axis bisects the square. The Fe ions were coordinated by three cyanide carbon donors and a tridentate tp* ligand. The Co ions were coordinated by the bidentate dtbbpy ligands and bridged to the Fe ions via the nitrogen donors of the cyanide groups. The Fe centers had an average coordination bond length of 1.959 Å at 100 K, characteristic of LS Fe^{II} or LS Fe^{III}, while the Co ions had bonding distances in the range 1.892–1.944 Å, indicative of LS Co^{III}.

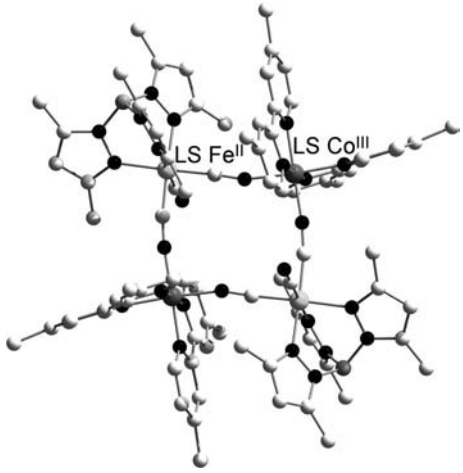

Figure 9. Diagram of $[Co_2Fe_2$-1] at 100 K; the dtbbpy *tert*-butyl groups have been omitted for clarity.

Magnetic susceptibility measurements conducted between 5 and 330 K showed constant χ_mT values below 250 K, at which point the χ_mT value was 0.18 emu mol^{-1} K, suggesting that $[Co_2Fe_2$-1] was in the diamagnetic electronic state of $[LSFe^{II}{}_2LSCo^{III}{}_2]$; the low-temperature (LT) phase, albeit with a slight paramagnetic impurity (Figure 10). Subsequent temperature increase from 250 to 330 K brought about a two-step increase in χ_mT value, with steps centered at 275 and 310 K, indicating the occurrence of ETCST from the LT to a high-temperature (HT) phase via an intermediate (IM) state. The χ_mT value at 330 K (HT phase) was 6.55 emu mol^{-1} K, in agreement with the expected Curie constant (6.32 emu mol^{-1} K) for the $[LSFe^{III}{}_2HSCo^{II}{}_2]$ electronic state of two isolated LS Fe^{III} (S = 1/2, g = 2.7) and two HS Co^{II} (S = 3/2, g = 2.3) ions. The χ_mT value of the IM phase was 3.33 emu mol^{-1} K at 296 K, half that of the HT phase.

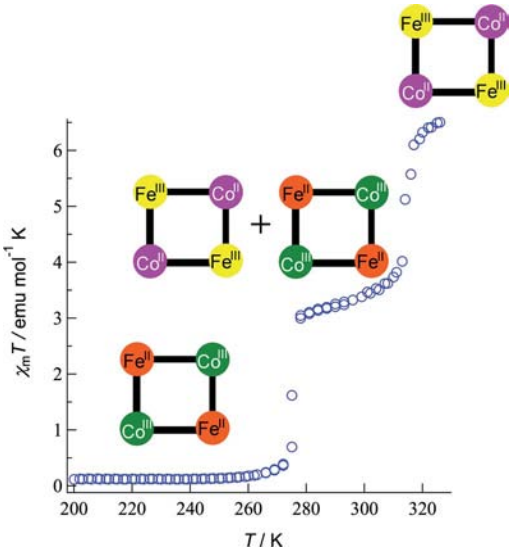

Figure 10. Magnetic susceptibility data collected for $[Co_2Fe_2$-1] displayed between 200 and 330 K, with schematics representing the spin transition in the squares. Orange circles represent Fe^{II} ions, green Co^{III}, yellow Fe^{III}, magenta Co^{II}.

^{57}Fe Mössbauer spectra of $[Co_2Fe_2$-1] were measured at 20, 280, and 320 K to determine the electronic states of the iron ions in the HS, IM, and LT phases (Figure 11). The measurements confirmed that all iron ions were in the LS Fe^{II} state in the LT phase, (δ = 0.22 and ΔE_Q = 0.43 mm s^{-1}) and in the oxidized LS Fe^{III} state in the HT phase (δ = 0.00 and ΔE_Q = 0.91 mm s^{-1}). The observation of the difference between the LT and HT phases indicates that complete ETCST from the [LS $Fe^{II}{}_2$ LS $Co^{III}{}_2$] to the [LS $Fe^{III}{}_2$ HS $Co^{II}{}_2$] state had occurred by 320 K. The IM phase displayed a 50:50 mixture of both doublets, suggesting that half of the iron ions had undergone ETCST at 280 K.

X-ray structural analyses conducted at temperatures corresponding to the IM and HT phases showed that the crystallographic space groups remained the same (*C*2/*c*), but that the bonding distances around the metal ions changed markedly. In the HT phase the Co and Fe ions had average bonding distances of 2.113 and 1.964 Å, respectively, suggesting complete ETCST from the LT phase to the HT phase. In contrast, the IM phase showed Co bonding distances with an average length of 2.020 Å, lying between those expected for HS Co^{II} and LS Co^{III} ions, suggesting positional disorder between HS and LS ions. Thus, there were two possibilities: firstly, that the IM phase contained $[Fe^{II}Fe^{III}Co^{II}Co^{III}]$ squares or secondly, that it consisted of a mixture of squares in their LT $[Fe^{II}{}_2Co^{III}{}_2]$ and HT $[Fe^{III}{}_2Co^{II}{}_2]$ states. To elucidate the nature of the IM phase, synchrotron radiation was employed at 298 K, which showed that, while the unit cell had maintained the same symmetry, it had quadrupled in volume to contain four crystallographically unique squares. Inspection of this data confirmed that the unit cell contained two [LS$Fe^{II}{}_2$-

 © 2011 Wiley-VCH Verlag GmbH & Co. KGaA, Weinheim

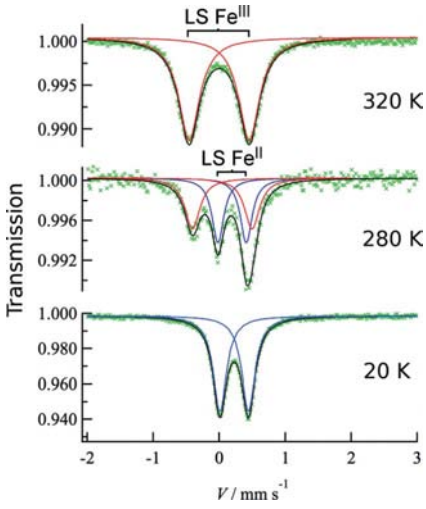

Figure 11. Mossbauer spectra of $[Co_2Fe_2\text{-}1]$ collected at 20, 280, and 320 K showing observed (green crosses), fit (black lines), LS Fe^{II} (blue lines), and LS Fe^{III} doublets (red lines). Velocity (V) is relative to metallic iron.

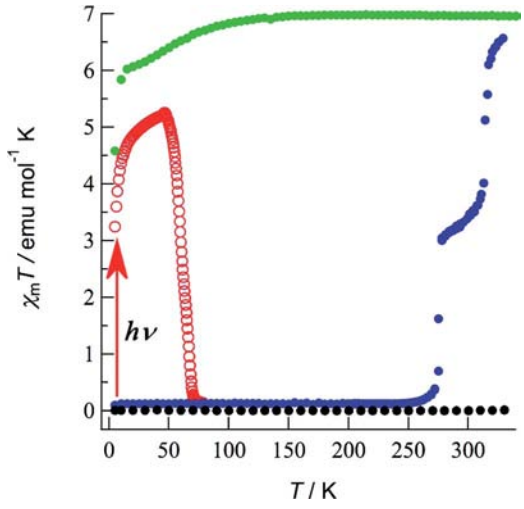

Figure 12. Magnetic susceptibility data collected for $[Co_2Fe_2\text{-}1]$ (blue), $[Co_2Fe_2\text{-}2]$ (green), and $[Co_2Fe_2\text{-}3]$ (black) between 5 and 330 K, the red rings show the effect of light irradiation (3 h, at 808 nm) of the LT phase of $[Co_2Fe_2\text{-}1]$.

$LSCo^{III}{}_2]$ and two $[LSFe^{III}{}_2HSCo^{II}{}_2]$ squares, which formed π-stacked layers in which the HT and LT species were alternately arranged.[50]

To investigate the importance of the choice of ligands used in the syntheses of ETCST-active clusters the dtbbpy and tp* ligands used in $[Fe_2Co_2\text{-}1]$ were replaced by bpy and tp ligands to give $[Co_2Fe_2(CN)_6(tp^*)_2(bpy)_4](PF_6)_2$ ($[Fe_2Co_2\text{-}2]$) and $[Co_2Fe_2(CN)_6(tp)_2(dtbbpy)_4](PF_6)_2$ ($[Fe_2Co_2\text{-}3]$), respectively. Derivatization of ligands with electron-donating substituents such as the methyl and *tert*-butyl groups in tp* and dtbbpy, respectively, changes the redox potentials of their coordinated metal ions. It was shown that, by using bpy in place of dtbbpy (in $[Fe_2Co_2\text{-}2]$), the cluster could be stabilized in the HT phase across the entire temperature range (Figure 12). In contrast, when tp was used in place of tp* (in $[Fe_2Co_2\text{-}3]$), the cluster was diamagnetic at all temperatures measured. These experiments emphasized the need for balance in the electron-donating character of the ligands used. If the difference in Gibbs free energy (ΔG) between the HT and LT phases is large, then the cluster will exist in one phase across the temperature range. Using a balanced choice of ligands minimizes ΔG and introduces the potential for the occurrence of ETCST.[50]

A phenomenon which has also been observed in all reported ETCST-active cyanide-bridged molecular squares is the potential to access a metastable phase at low temperatures, through light-induced ETCST (LIETCST). Light irradiation at wavelengths close to that of the IVCT band for the $Fe^{II}\rightarrow Co^{III}$ transition in $[Co_2Fe_2\text{-}1]$ (λ_{max} = 770 nm in butyronitrile) at 5 K led to a sharp increase of χ_mT up to a saturated value of 3.25 emu mol^{-1} K after 3 hours of irradiation, indicating the generation of a light-induced HT phase, (Figure 11). The light source was then removed, and the temperature was increased, which caused the χ_mT values to climb steadily to a maximum of 5.25 emu mol^{-1} K at 46 K, approximately 80% of the value observed for the HT phase at 330 K, a disparity put down to the incomplete light penetration of the crystals. Above 46 K the light-induced HT phase thermally relaxed and had fully returned to the LT diamagnetic phase by 80 K. Interestingly, the differential plot of the transition showed that the thermal relaxation of the light-induced HT phase was a two-step phenomenon, passing through an intermediate state at approximately half of the maximum χ_mT value for the light-induced phase, suggesting that it may be the same mixed electronic state as that observed in the thermal IM state.

In 2010, Lescouëzec's group reported the synthesis of an $[Fe_2Co_2]$ square in which the square was in the diamagnetic $[Fe^{II}{}_2Co^{III}{}_2]$ state across the entire temperature range measured.[51] However, when the samples were irradiated with white halogen light at 10 K for a period of 4 hours, a paramagnetic signal appeared that was saturated at 7.2 emu mol^{-1} K, indicative of the occurrence of photoinduced electron transfer and a change in the complex from the diamagnetic state to a metastable light-induced paramagnetic phase, $[Fe^{III}{}_2Co^{II}{}_2]$. After the light source was removed, the temperature was gradually increased, and this led to an initial slight decrease in χ_mT up to 35 K, after which χ_mT remained almost constant until around 100 K, when the metastable phase thermally relaxed back to the native diamagnetic state. The magnetic behavior suggested that full transition had occurred and that the light-induced $[Fe^{III}{}_2Co^{II}{}_2]$ state had ferromagnetic interactions between all metal centers. This type of light-induced diamagnetic → ferromagnetic switching may be an important target in the future development of molecular devices and quantum computing.[51]

Conclusions

This review has introduced the recent developments in the field of cyanide-bridged molecular square complexes.

 © 2011 Wiley-VCH Verlag GmbH & Co. KGaA, Weinheim

These molecules are an attractive synthetic target and can be controllably generated from a number of building block approaches, and they can be relatively easily tuned to be homo- or heterometallic. Likewise, their physical properties, such as the spin ground state, can be controlled by the choice of constituents. Their properties are varied and generally relate back to the behavior of cyanide bridges as facilitators of electronic and magnetic coupling interactions. Multiple oxidation and spin states can be stabilized in the squares as a result of their rigidity, and recent work on SCO- and ETCST-active species has suggested that these could be key materials in the development of new molecular devices. Indeed, $[Fe_2Co_2]$ squares have recently shown multistep ETCST behavior and light-induced bistable magnetic states at low temperatures.

Acknowledgments

This work was supported by a Grant-in-Aid for Scientific Research and for Priority Area "Coordination Programming" (Area 2107) from the Ministry of Education, Culture, Sports, Science and Technology (MEXT), Japan and the Japan Society for the Promotion of Science (JSPS).

[1] J. Woodward, *Philos. Trans. R. Soc. London* **1724**, *33*, 15–17.
[2] A. Ito, M. Suenaga, K. Ôno, *J. Chem. Phys.* **1968**, *48*, 3597–3599.
[3] S. Ferlay, T. Mallah, R. Ouahès, P. Veillet, M. Verdaguer, *Nature* **1995**, *378*, 701–703.
[4] a) K. R. Dunbar, R. A. Heintz, *Prog. Inorg. Chem.* **1997**, *45*, 283–391 and references cited therein; b) M. Verdaguer, A. Bleuzen, V. Marvaud, J. Vaissermann, M. Seuleima, C. Desplanches, A. Scuiller, C. Train, R. Garde, G. Gelly, C. Lomenech, I. Rosenman, P. Veillet, C. Cartier, F. Villain, *Coord. Chem. Rev.* **1999**, *190–192*, 1023–1047, and references cited therein; c) M. Verdaguer, *Science* **1996**, *272*, 698–699; d) W. Kosaka, K. Nomura, K. Hashimoto, S. Ohkoshi, *J. Am. Chem. Soc.* **2005**, *127*, 8590–8591; e) W. E. Buschmann, J. Ensling, P. Gütlich, J. S. Miller, *Chem. Eur. J.* **1999**, *5*, 3019–3028; f) S. Ohkoshi, H. Tokoro, T. Matsuda, H. Takahashi, H. Irie, K. Hashimoto, *Angew. Chem.* **2007**, *119*, 3302; *Angew. Chem. Int. Ed.* **2007**, *46*, 3238–3241; g) K. Itaya, I. Uchida, V. Neff, *Acc. Chem. Res.* **1986**, *19*, 162–168; h) S. Ohkoshi, A. Fujishima, K. Hashimoto, *J. Am. Chem. Soc.* **1998**, *120*, 5349–5350; i) S. S. Kaye, J. R. Long, *J. Am. Chem. Soc.* **2005**, *127*, 6506–6507.
[5] a) J. L. Heinrich, P. A. Berseth, J. R. Long, *Chem. Commun.* **1998**, 1231–1232; b) K. K. Klausmeyer, T. B. Rauchfuss, S. R. Wilson, *Angew. Chem.* **1998**, *110*, 1808; *Angew. Chem. Int. Ed.* **1998**, *37*, 1694–1696; c) K. K. Klausmeyer, S. R. Wilson, T. B. Rauchfuss, *J. Am. Chem. Soc.* **1999**, *121*, 2705–2711; d) D. Li, S. Parkin, G. Wang, G. T. Yee, R. Clérac, W. Wernsdorfer, S. M. Holmes, *J. Am. Chem. Soc.* **2006**, *128*, 4214–4215; e) Z.-G. Gu, W. Liu, Q.-F. Yang, X.-H. Zhou, J.-L. Zuo, X.-Z. You, *Inorg. Chem.* **2007**, *46*, 3236–3244; f) D. Li, S. Parkin, R. Clérac, S. M. Holmes, *Inorg. Chem.* **2006**, *45*, 7569–7571; g) E. J. Schelter, F. Karadas, C. Avendano, A. V. Prosvirin, W. Wernsdorfer, K. R. Dunbar, *J. Am. Chem. Soc.* **2007**, *129*, 8139–8149; h) Z.-G. Gu, W. Liu, Q.-F. Yang, X.-H. Zhou, J.-L. Zuo, X.-Z. You, *Inorg. Chem.* **2007**, *46*, 3236–3244; i) M. Nihei, M. Ui, N. Hoshino, H. Oshio, *Inorg. Chem.* **2008**, *47*, 6106–6108.
[6] M. Shatruk, C. Avendano, K. R. Dunbar, "Cyanide-Bridged Complexes of Transition Metals: A Molecular Magnetism Perspective" in *Progress in Inorganic Chemistry* (Ed.: K. D. Karlin), John Wiley & Sons, Inc., Hoboken, New Jersey, **2009**, vol. 56, pp. 155–334.
[7] P. Schinnerling, U. Thewalt, *J. Organomet. Chem.* **1992**, *431*, 41–45.
[8] H. Oshio, O. Tamada, H. Onodera, T. Ito, T. Ikoma, S. Tero-Kubota, *Inorg. Chem.* **1999**, *38*, 5686–5689.
[9] J. L. Boyer, M. L. Kuhlman, T. B. Rauchfuss, *Acc. Chem. Res.* **2007**, *40*, 233–242.
[10] H. Oshio, H. Onodera, O. Tamada, H. Mizutani, T. Hikichi, T. Ito, *Chem. Eur. J.* **2000**, *6*, 2523–2530.
[11] H. Oshio, H. Onodera, T. Ito, *Chem. Eur. J.* **2003**, *9*, 3946–3950.
[12] M. L. Flay, V. Comte, H. Vahrenkamp, *Z. Anorg. Allg. Chem.* **2003**, *629*, 1147–1152.
[13] M. Nihei, M. Ui, M. Yokota, L. Han, A. Maeda, H. Kishida, H. Okamoto, H. Oshio, *Angew. Chem.* **2005**, *117*, 6642; *Angew. Chem. Int. Ed.* **2005**, *44*, 6484–6487.
[14] J.-N. Rebilly, L. Catala, G. Charron, G. Rogez, E. Rivière, R. Guillot, P. Thuéry, A.-L. Barra, T. Mallah, *Dalton Trans.* **2006**, 2818–2828.
[15] a) J. Kim, S. Han, I.-K. Cho, K. Y. Choi, M. Heu, S. Yoon, B. J. Suh, *Polyhedron* **2004**, *23*, 1333–1339; b) D.-Y. Wu, O. Sato, C.-Y. Duan, *Inorg. Chem. Commun.* **2009**, *12*, 325–327; c) M. Tang, D. Li, U. P. Mallik, J. R. Withers, S. Brauer, M. R. Rhodes, R. Clérac, G. T. Yee, M.-H. Whangbo, S. M. Holmes, *Inorg. Chem.* **2010**, *49*, 4753–4755.
[16] F. Li, J. K. Clegg, L. Goux-Capes, G. Chastanet, D. M. D'Alessandro, J.-F. Létard, C. J. Kepert, *Angew. Chem. Int. Ed.* **2011**, *50*, 2820–2823.
[17] a) D. Li, S. Parkin, G. Wang, G. T. Yee, A. V. Prosvirin, S. M. Holmes, *Inorg. Chem.* **2005**, *44*, 4903–4905; b) D. Li, S. Parkin, G. Wang, G. T. Yee, S. M. Holmes, *Inorg. Chem.* **2006**, *45*, 1951–1959.
[18] A. Rodríguez-Diéguez, R. Kivekäs, R. Sillanpää, J. Cano, F. Lloret, V. McKee, H. Stoeckli-Evans, E. Colacio, *Inorg. Chem.* **2006**, *45*, 10537–10551.
[19] a) Z.-X. Wang, X.-L. Li, T.-W. Wang, Y.-Z. Li, S. Ohkoshi, K. Hashimoto, Y. Song, X.-Z. You, *Inorg. Chem.* **2007**, *46*, 10990–10995; b) H. Zhao, M. Shatruk, A. V. Prosvirin, K. R. Dunbar, *Chem. Eur. J.* **2007**, *13*, 6573–6589; c) T. S. Venkatakrishnan, C. Desplanches, R. Rajamani, P. Guionneau, L. Ducasse, S. Ramasesha, J.-P. Sutter, *Inorg. Chem.* **2008**, *47*, 4854–4860; d) T. Korzeniak, C. Desplanches, R. Podgajny, C. Giménez-Saiz, K. Stadnicka, M. Rams, B. Sieklucka, *Inorg. Chem.* **2009**, *48*, 2865–2872; e) R. Podgajny, T. Korzeniak, P. Przychodzeń, C. Giménez-Saiz, M. Rams, M. Kwaśniak, B. Sieklucka, *Eur. J. Inorg. Chem.* **2010**, 4166–4174.
[20] L. Jiang, T.-B. Lu, X.-L. Feng, *Inorg. Chem.* **2005**, *44*, 7056–7062.
[21] L. R. Falvello, M. Tomás, *Chem. Commun.* **1999**, 273–274.
[22] a) C. P. Berlinguette, J. A. Smith, J. R. Galán-Mascarós, K. R. Dunbar, *C. R. Chim.* **2002**, *5*, 665–672; b) L. M. Toma, R. Lescouëzec, D. Cangussu, R. Llusar, J. Mata, S. Spey, J. A. Thomas, F. Lloret, M. Julve, *Inorg. Chem. Commun.* **2005**, *8*, 382–385.
[23] a) K. K. Klausmeyer, T. B. Rauchfuss, S. R. Wilson, *Angew. Chem.* **1998**, *110*, 1808; *Angew. Chem. Int. Ed.* **1998**, *37*, 1694–1696; b) D. J. Darensbourg, W.-Z. Lee, M. J. Adams, D. L. Larkins, J. H. Reibenspies, *Inorg. Chem.* **1999**, *38*, 1378–1379; c) D. J. Darensbourg, M. J. Adams, J. C. Yarbrough, *Inorg. Chem.* **2001**, *40*, 6543–6544; d) D. J. Darensbourg, W.-Z. Lee, M. J. Adams, J. C. Yarbrough, *Eur. J. Inorg. Chem.* **2001**, 2811–2822; e) D. J. Darensbourg, M. J. Adams, J. C. Yarbrough, A. L. Phelps, *Eur. J. Inorg. Chem.* **2003**, 3639–3648; f) D. J. Darensbourg, M. J. Adams, J. C. Yarbrough, A. L. Phelps, *Inorg. Chem.* **2003**, *42*, 7809–7818; g) D. J. Darensbourg, A. L. Phelps, *Inorg. Chim. Acta* **2004**, *357*, 1603–1607.
[24] J. Forniés, J. Gómez, E. Lalinde, M. T. Moreno, *Chem. Eur. J.* **2004**, *10*, 888–898.

 © 2011 Wiley-VCH Verlag GmbH & Co. KGaA, Weinheim

[25] a) F. Olbrich, J. Kopf, E. Weiss, *J. Organomet. Chem.* **1993**, *456*, 293–298; b) S. M. Contakes, T. B. Rauchfuss, *Angew. Chem.* **2000**, *112*, 2060; *Angew. Chem. Int. Ed.* **2000**, *39*, 1984–1986; c) J. P. H. Charmant, P. Espinet, K. Soulantica, *Acta Crystallogr., Sect. E* **2001**, *57*, 451–453.

[26] a) G. S. Hanan, D. Volkmer, J.-M. Lehn, *Can. J. Chem.* **2004**, *82*, 1428–1434; b) M. Ruben, J. Rojo, F. J. Romero-Salguero, L. H. Uppadine, J.-M. Lehn, *Angew. Chem.* **2004**, *116*, 3728; *Angew. Chem. Int. Ed.* **2004**, *43*, 3644–3662; c) L. H. Uppadine, J.-P. Gisselbrecht, N. Kyritsakas, K. Naettinen, K. Rissanen, J.-M. Lehn, *Chem. Eur. J.* **2005**, *11*, 2549–2565; d) V. A. Milway, S. M. T. Abedin, V. Niel, T. L. Kelly, L. N. Dawe, S. K. Dey, D. W. Thompson, D. O. Miller, M. S. Alam, P. Mueller, L. K. Thompson, *Dalton Trans.* **2006**, 2835–2851; e) T. Shiga, T. Matsumoto, M. Noguchi, T. Onuki, N. Hoshino, G. N. Newton, M. Nakano, H. Oshio, *Chem. Asian J.* **2009**, *4*, 1660–1663.

[27] a) C. Creutz, H. Taube, *J. Am. Chem. Soc.* **1969**, *91*, 3988–3989; b) C. Creutz, H. Taube, *J. Am. Chem. Soc.* **1973**, *95*, 1086–1094.

[28] a) D. M. D'Alessandro, F. R. Keene, *Chem. Rev.* **2006**, *106*, 2270–2298; b) K. D. Demadis, C. M. Hartshorn, T. J. Meyer, *Chem. Rev.* **2001**, *101*, 2655–2685.

[29] a) J. Jiao, G. J. Long, L. Rebbouh, F. Grandjean, A. M. Beatty, T. P. Fehler, *J. Am. Chem. Soc.* **2005**, *127*, 17819–17831; b) Y. Zhao, D. Guo, Y. Liu, C. He, Z. Lin, C. Duan, *Chem. Commun.* **2008**, 5725–5727.

[30] M. B. Robin, P. Day, *Adv. Inorg. Chem. Radiochem.* **1967**, *10*, 247–422.

[31] a) N. S. Hush, *Prog. Inorg. Chem.* **1967**, *8*, 391–444; b) C. Creutz, *Prog. Inorg. Chem.* **1983**, *30*, 1–73.

[32] J. B. Goodenough *Magnetism and the Chemical Bond* (Ed.: F. A. Cotton), John Wiley & Sons, New York, **1963**, pp. 1–393.

[33] a) W. Liu, C.-F. Wang, Y.-Z. Li, J.-L. Zuo, X.-Z. You, *Inorg. Chem.* **2006**, *45*, 10058–10065; b) H.-R. Wen, C.-F. Wang, Z.-Y. Du, J.-L. Zuo, *Inorg. Chim. Acta* **2008**, *361*, 2901–2908.

[34] a) D. Li, R. Clérac, G. Wang, G. T. Yee, S. M. Holmes, *Eur. J. Inorg. Chem.* **2007**, 1341–1346; b) C.-F. Wang, W. Liu, Y. Song, X.-H. Zhou, J.-L. Zuo, X.-Z. You, *Eur. J. Inorg. Chem.* **2008**, 717–727; c) D. Wu, Y. Zhang, W. Huanga, O. Sato, *Dalton Trans.* **2010**, *39*, 5500–5503; d) Y.-H. Peng, Y.-F. Meng, L. Hu, Q.-X. Li, Y.-Z. Li, J.-L. Zuo, X.-Z. You, *Inorg. Chem.* **2010**, *49*, 1905–1912; e) N. Hoshino, Y. Sekine, M. Nihei, H. Oshio, *Chem. Commun.* **2010**, *46*, 6117–6119.

[35] a) F. Karadas, E. J. Schelter, M. Shatruk, A. V. Prosvirin, J. Bacsa, D. Smirnov, A. Ozarowski, J. Krzystek, J. Telser, K. R. Dunbar, *Inorg. Chem.* **2008**, *47*, 2074–2082; b) F. Karadas, E. J. Schelter, A. V. Prosvirin, J. Bacsa, K. R. Dunbar, *Chem. Commun.* **2005**, 1414–1416; c) F. Karadas, M. Shatruk, L. M. Perez, K. R. Dunbar, *Chem. Eur. J.* **2010**, *16*, 7164–7173.

[36] a) K. Harada, J. Yuzurihara, Y. Ishii, N. Sato, H. Kambayashi, Y. Fukuda, *Chem. Lett.* **1995**, 887–888; b) H.-Z. Kou, S. Gao, C.-H. Li, D.-Z. Liao, B.-C. Zhou, R.-J. Wang, Y. Li, *Inorg. Chem.* **2002**, *41*, 4756–4762; c) Y.-F. Huang, H.-H. Wei, M. Katada, *J. Coord. Chem.* **2008**, *61*, 2683–2689.

[37] H. Oshio, M. Yamamoto, T. Ito, *Inorg. Chem.* **2002**, *41*, 5817–5820.

[38] K. Park, S. M. Holmes, *Phys. Rev. B* **2006**, *74*, 224440–1–10.

[39] a) P. Gütlich, A. Hauser, H. Spiering, *Angew. Chem.* **1994**, *106*, 2109; *Angew. Chem. Int. Ed. Engl.* **1994**, *33*, 2024–2054; b) O. Kahn, C. J. Martinez, *Science* **1998**, *279*, 44–48; c) P. Gütlich, Y. Garcia, T. Woike, *Coord. Chem. Rev.* **2001**, *219–221*, 839–879; d) T. Sato, K. Nishi, S. Iijima, M. Kojima, N. Matsumoto, *Inorg. Chem.* **2009**, *48*, 7211–7229.

[40] M. Nihei, M. Ui, H. Oshio, *Polyhedron* **2009**, *28*, 1718–1721.

[41] I. Boldog, F. J. Muñoz-Lara, A. B. Gaspar, M. C. Muñoz, M. Seredyuk, J. A. Real, *Inorg. Chem.* **2009**, *48*, 3710–3719.

[42] E. M. Zueva, E. R. Ryabikh, A. M. Kuznetsov, S. A. Borshch, *Inorg. Chem.* **2011**, *50*, 1905–1913.

[43] N. Shimamoto, S. Ohkoshi, O. Sato, K. Hashimoto, *Inorg. Chem.* **2002**, *41*, 678–684.

[44] a) O. Sato, T. Lyoda, A. Fujishima, K. Hashimoto, *Science* **1996**, *272*, 704–705; b) O. Sato, Y. Einaga, T. Iyoda, A. Fujishima, K. Hashimoto, *J. Electrochem. Soc.* **1997**, *144*, L11–L13.

[45] a) C. P. Berlinguette, A. Dragulescu-Andrasi, A. Sieber, J. R. Galán-Mascarós, H. U. Güdel, C. Achim, K. R. Dunbar, *J. Am. Chem. Soc.* **2004**, *126*, 6222–6223; b) C. P. Berlinguette, A. Dragulescu-Andrasi, A. Sieber, H. U. Güdel, C. Achim, K. R. Dunbar, *J. Am. Chem. Soc.* **2005**, *127*, 6766–6779; c) M. Shatruk, A. Dragulescu-Andrasi, K. E. Chambers, S. A. Stoian, E. L. Bominaar, C. Achim, K. R. Dunbar, *J. Am. Chem. Soc.* **2007**, *129*, 6104–6116.

[46] M. G. Hilfiger, M. Chen, T. V. Brinzari, T. M. Nocera, M. Shatruk, D. T. Petasis, J. L. Musfeldt, C. Achim, K. R. Dunbar, *Angew. Chem.* **2010**, *122*, 1452; *Angew. Chem. Int. Ed.* **2010**, *49*, 1410–1413.

[47] D. Li, R. Clérac, O. Roubeau, E. Harté, C. Mathonière, R. Le Bris, S. M. Holmes, *J. Am. Chem. Soc.* **2008**, *130*, 252–258.

[48] Y. Zhang, D. Li, R. Clérac, M. Kalisz, C. Mathonière, S. M. Holmes, *Angew. Chem. Int. Ed.* **2010**, *49*, 3752–3756.

[49] M. Nihei, Y. Sekine, N. Suganami, H. Oshio, *Chem. Lett.* **2010**, *39*, 978–979.

[50] M. Nihei, Y. Sekine, N. Suganami, K. Nakazawa, A. Nakao, H. Nakao, Y. Murakami, H. Oshio, *J. Am. Chem. Soc.* **2011**, *133*, 3592–3600.

[51] J. Mercurol, Y. Li, E. Pardo, O. Risset, M. Seuleiman, H. Rousselière, R. Lescouëzec, M. Julve, *Chem. Commun.* **2010**, *46*, 8995–8997.

Received: April 14, 2011
Published Online: June 10, 2011

 © 2011 Wiley-VCH Verlag GmbH & Co. KGaA, Weinheim